INTERNATIONAL JOURNAL OF ENERGY STUDIES

e-ISSN: 2717-7513 (ONLINE); homepage: https://dergipark.org.tr/en/pub/ijes

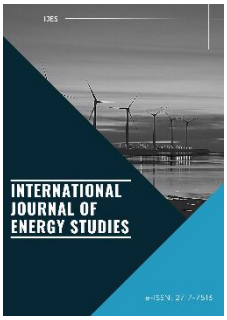

Research Article
Int J Energy Studies 2026; 11(1): 437-460
DOI: 10.58559/ijes.1861704

Received : 12 Jan 2026
Revised : 20 Feb 2026
Accepted : 23 Feb 2026

Effect of concave and convex side-wall curvature on natural convective heat transfer in trapezoidal enclosures

Çağatay Yıldız[a*]

[a]*Mechanical Engineering Department, Engineering Faculty, Kocaeli University, 41001, Kocaeli, Türkiye, ORCID : 0000-0002-1233-373X*

*(*Corresponding Author: cagatay.yildiz@kocaeli.edu.tr)*

Highlights

- The influence of concave and convex wall geometries on natural convection was systematically evaluated.
- Local vortices in concave enclosures restricted hot–cold mixing, reducing heat transfer by up to 45%.
- Convex enclosures promoted smoother circulation and improved hot-cold fluid mixing.
- The average Nusselt number increased by up to 18.6% with the use of convex enclosures.

You can cite this article as: Yıldız Ç. Effect of concave and convex side-wall curvature on natural convective heat transfer in trapezoidal enclosures. Int J Energy Studies 2026; 11(1): 437-460.

ABSTRACT

Focusing on the enhancement effects of fluid flow alteration on natural convective heat transfer in enclosures, this study presents a numerical investigation about natural convection behavior inside the concave and convex shaped trapezoidal-based enclosures. The side walls of a two-dimensional standard isosceles trapezoidal enclosure (TE) were modified to constitute concave and convex enclosures based on the reference geometry. Regarding the wall curvature, three different concave (C1, C2, and C3) and three different convex (V1, V2, and V3) enclosures were examined in terms of natural convective heat transfer, considering three different Rayleigh numbers (Ra=10^4, 10^5, and 10^6). The governing equations of the problem was solved by finite volume based commercial software, and the heat transfer performance was discussed over dimensionless streamline and temperature contours, as well as quantified by average Nusselt numbers (Nu). The numerical outcomes revealed that the curvature of side walls have significant effects on buoyancy-driven fluid flow and heat transfer. The fluid flow was squeezed and restricted in concave enclosures, particularly at high Ra, while double longitudinal circulations were generally formed in convex enclosures. Hence, utilization of concave enclosures led to a significant decrease in Nu, approaching 45%, while the convex-shaped enclosures resulted in a remarkable improvement in Nu, which can reach up to 18.6% depending on the Ra, compared to the reference enclosure. Regarding the outcomes of the work, convex-structured enclosures were found to be superior for enhancing heat transfer and were recommended for engineering applications such as cooling of electronics, solar thermal energy and relevant heat exchangers.

Keywords: Concave, Convex, Enclosure, Heat transfer enhancement, Natural convection

1. INTRODUCTION

A vast array of thermal engineering applications involve natural convection due to its suitability and minimal external energy requirement [1], as well as being an essential heat transfer mechanism [2]. Free convective heat transfer can be commonly integrated with various industrial processes such as cooling of electronics [3], solar thermal collectors [4], heat exchangers [5] and various thermal energy storage units [6]. Various two- and three-dimensional enclosure models are suitable for modeling the fluid flow and heat transfer behavior in these systems, and they are frequently considered by researchers [7].

Efficient operation of such thermal systems is highly influenced by the effectiveness of free convective heat transfer, which depends on many factors related to Grashof (*Gr*) and Prandtl numbers (*Pr*) [8]. Apart from these two dimensionless parameters including various physical properties and effects, geometrical constraints such as enclosure shape [9,10] and inclination [11] as well as additional heat transfer enhancement techniques, such as nanoparticle addition [12] and fin attachment [13]. Even though these techniques can be implemented in combination [14], geometrical variations can be significantly effective as a heat transfer enhancement technique in addition to their cost-effectiveness, compared to other methods.

By the growing needs for effective heat exchange in thermal systems, research focusing on heat transfer enhancement in various enclosures hosting free convection has been recently accelerated [15]. Aside from conventional square or rectangular geometries, TEs have been reported to be more suitable for some special cooling and heat exchanger applications dealing with electronic components, solar absorbers and water heating systems, etc. [16–18]. Furthermore, it has been stated that the free convective heat transfer in TEs is a more challenging phenomenon, due to the presence of inclined walls and a narrowing or expanding flow area, compared to the heat transfer behavior in classical square or rectangular enclosures [19,20].

To overcome the challenges mentioned in the previous paragraph and contribute to improvement of heat transfer in TEs, researchers have exhibited a significant effort throughout the last decade. Free convective heat transfer in a TE with stratification was numerically investigated by Rahaman et al. [21], and the authors reported the observations of Pitchfork and Hopf bifurcation structures depending on the investigated *Ra*, and the free convective flow structure became chaotic for *Ra* beyond 4×10^7. Bilal et al. [22] explored natural convection heat transfer in a TE containing a non-

Newtonian power-law fluid and a centrally placed U-shaped fin, considering the rheological influences. The authors analyzed flow and temperature fields over a range of Ra=10^4 to 10^6 and power-law indices between 0.5 and 1.5. Results showed that increasing the *Ra* enhances momentum and heat transfer, while higher power-law indices, i.e., more viscous behavior, suppress them. Considering various engineering applications involving fluid-solid interaction, Mehryan et al. [23] conducted a numerical work investigating the natural convection in a TE which includes a flexible partition. The increase in *Ra* led to higher forces on the flexible partition, resulting in higher tension consequently. The comparisons to the square cavity revealed that the rate of heat transfer can increase up to 15% in square enclosure, compared to the trapezoidal one, i.e., the inclined side walls. Yet, the inclined wall impact on the tension of the flexible partition was found to be slight.

A conductive object constituting a full and part of a circular shape was introduced in a TE filled with nanofluid by Selimefendigil [24], and the impact of different shapes of the conductive obstacle as well as the shapes of nanoparticles have been investigated thoroughly, for different nanoparticle fractions, side wall inclinations, and thermal conductivity ratios. The study revealed that the thermal conductivity ratio has insignificant effect on the heat transfer rate, while the highest improvements (13% to 16%) in the heat transfer were attained by using cylindrical nanoparticles, instead of spherical ones. Another geometric modification recently implemented to TE involved the placement of corrugated structure onto the heated wall [25]. The authors reported that the triangular corrugation provided the highest overall thermal performance ratio, especially when it is combined with dry concrete at low *Ra*.

As can be explicitly inferred from the present literature survey, geometrical modifications may significantly enhance heat transfer provided that they are implemented cautiously. This, of course, requires attentive parametric study in order to figure out which cases and combinations yield an enhanced and effective heat transfer. Building upon these deductions, this study aims at investigating the impact of wall curvature of TEs on the natural convective flow structure and heat transfer. Therefore, six different wall curvatures, namely three for convex and three for concave structures, were implemented on an isosceles TE and investigated within this study in means of free convection enhancement. The results were benchmarked with the original isosceles trapezoidal cavity, i.e., no curved walls (reference case), in order to quantify the relevant influences. Additionally, the study has been conducted considering three different Rayleigh

numbers (Ra=10^4, 10^5, and 10^6) to elaborate the geometrical impacts at different magnitude levels of free convective flow. The outcomes have been presented in terms of dimensionless streamline and temperature contours, as well as average Nusselt numbers, comparatively.

2. MATERIAL AND METHODS

2.1. Problem Description

The reference model, namely the standard isosceles TE is shown in Figure 1 together with its relevant dimension symbolizations. The bottom and top walls of the enclosure have a length of L and $L/2$, respectively, while its height is denoted by H. Furthermore, Figure 2 illustrates the geometrically modified enclosures, i.e., the TEs with curved walls in a concave and convex way, separately, at different curvatures. The curvatures of the walls are mathematically defined via parametric functions, which are given in the upcoming paragraphs.

Three different curvatures were considered in the numerical simulations for the concave and the convex structures each. Hence, apart from the reference benchmark enclosure of TE, six different enclosures were included in the study. The concave structures are named as C1, C2, and C3 in the order of increasing curvature, while the convex structures are similarly denoted by V1, V2, and V3, as previously given in Figure 2. Additionally, the parametric functions mathematically defining the curvatures of the aforementioned concave and convex enclosures were summarized in Table 1. The lengths of the bottom and top wall are denoted by L_1 and L_2, while the enclosure height is symbolized by H.

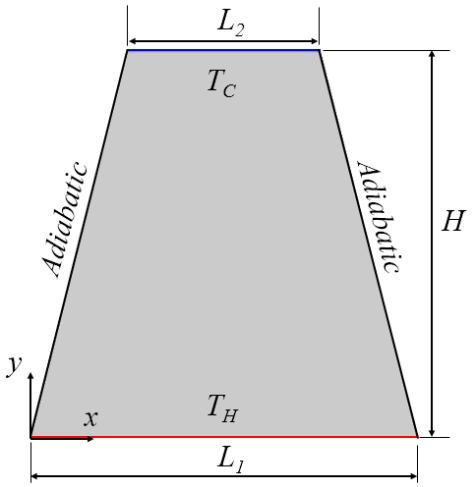

Figure 1. The isosceles trapezoidal enclosure with relevant dimensions and boundary conditions

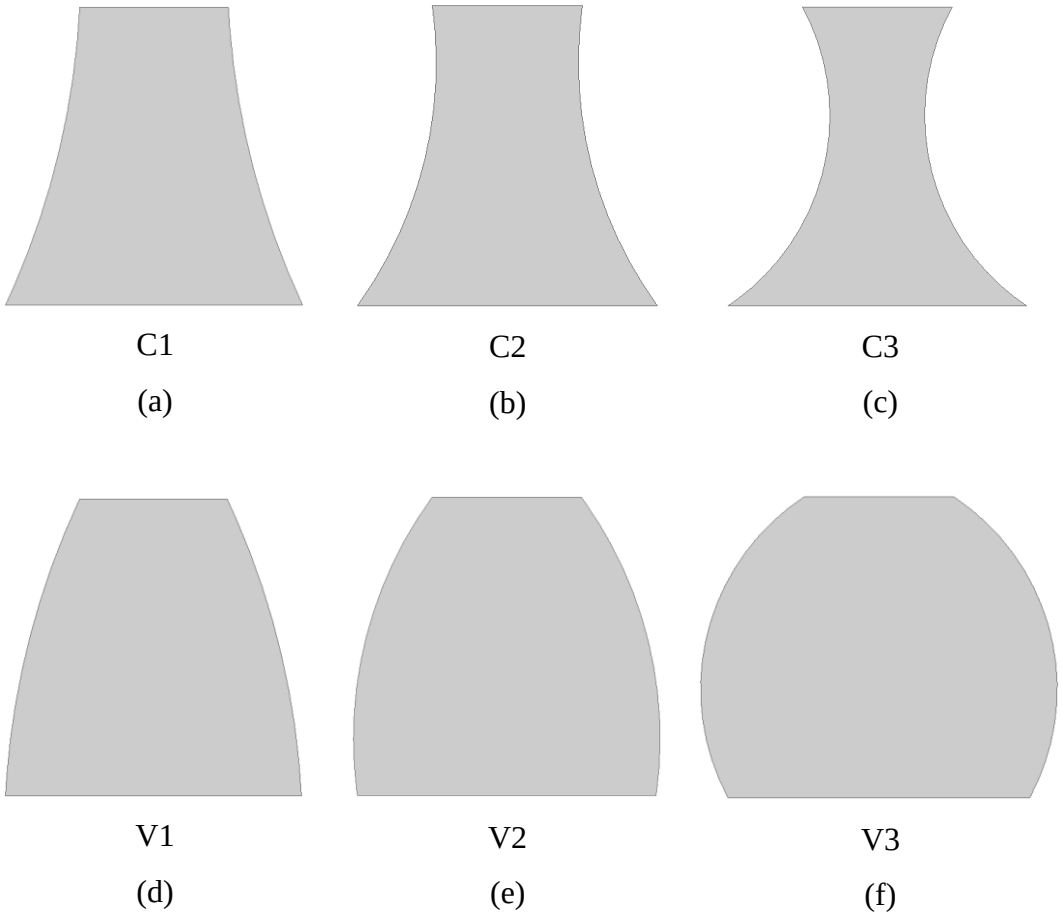

Figure 2. Schematic illustration of the concave (a, b, c) and the convex (d, e, f) enclosures together with their abbreviations

Table 1. Parametric functions for the definition of wall curvatures

Cavity code	Relevant parametric equation for the wall curvature	Equation number
C1	$x = -2.927 + 2.681 * \cos(-0.438402 + t * 0.386846)$ $y = 1.138 + 2.681 * \sin(-0.438402 + t * 0.386846)$	(1)
C2	$x = -1.615 + 1.378 * \cos(-0.628273 + t * 0.766589)$ $y = 0.810 + 1.378 * \sin(-0.628273 + t * 0.766589)$	(2)
C3	$x = -0.922 + 0.764 * \cos(-0.985316 + t * 1.480674)$ $y = 0.637 + 0.764 * \sin(-0.985316 + t * 1.480674)$	(3)
V1	$x = 2.178 + 2.681 * \cos\big(3.090037 + t * (-0.386846)\big)$ $y = -0.138 + 2.681 * \sin\big(3.090037 + t * (-0.386846)\big)$	(4)
V2	$x = 0.865 + 1.378 * \cos\big(-3.003277 + t * (-0.766589)\big)$	(5)

	$y = 0.190 + 1.378 * \sin(-3.003277 + t * (-0.766589))$	
V3	$x = 0.172 + 0.764 * \cos(3.090956 + t * (-1.480674))$ $y = 0.363 + 0.764 * \sin(3.090956 + t * (-1.480674))$	(6)

Regarding Eqs. 1 to 6, the function parameter, *t*, is dependent on *x* and *y* coordinates and is defined as follows:

$$x(t) = x_c + R\cos(\varphi_0 + t\Delta\varphi) \qquad t \in [0,1] \tag{7}$$

$$y(t) = y_c + R\sin(\varphi_0 + t\Delta\varphi) \qquad t \in [0,1] \tag{8}$$

where R is the radius of the circle, i.e., the constant distance between the center (x_c, y_c) and any point on the arc, while φ is the polar angle about the center, and the *x* and *y* within the functions were in m. Besides, *t* is a dimensionless parameter in the interval [0,1] that linearly varies the angle from φ_0 to $\varphi_0 + \Delta\varphi$, thereby defining points along the arc.

The flow inside the enclosures was considered to be two-dimensional, laminar and steady state, while the fluid is taken as Newtonian where the thermophysical properties remained constant, except density, which is treated by Boussinesq approximation. The governing equations reflecting the physical structure of the free convection phenomenon inside the enclosures include continuity, momentum, and energy equations, which are respectively given in two-dimensional Cartesian coordinates as follows [26]:

$$\frac{\partial u}{\partial x} + \frac{\partial v}{\partial y} = 0 \tag{9}$$

$$u\frac{\partial u}{\partial x} + v\frac{\partial u}{\partial y} = \frac{1}{\rho}\left[-\frac{\partial p}{\partial x} + \mu\left(\frac{\partial^2 u}{\partial x^2} + \frac{\partial^2 u}{\partial y^2}\right)\right] \tag{10}$$

$$u\frac{\partial v}{\partial x} + v\frac{\partial v}{\partial y} = \frac{1}{\rho}\left[-\frac{\partial p}{\partial y} + \mu\left(\frac{\partial^2 v}{\partial x^2} + \frac{\partial^2 v}{\partial y^2}\right)\right] + g\beta(T - T_{ref}) \tag{11}$$

$$u\frac{\partial T}{\partial x} + v\frac{\partial T}{\partial y} = \alpha\left[\frac{\partial^2 T}{\partial x^2} + \frac{\partial^2 T}{\partial y^2}\right] \tag{12}$$

The symbols *u* and *v* in the given equations represent the velocity components in *x* and *y* directions, respectively. The thermophysical properties, namely the density, dynamic viscosity, thermal diffusivity, and thermal expansion coefficient, are denoted by ρ, μ, α, and β, respectively. Lastly, pressure, temperature, and gravitational acceleration are symbolized by *p*, *T*, and *g*, respectively. The aforementioned parameters in the governing equations were considered in non-dimensional format to improve the generalizability of the outcomes as well as applicability in a wide range of

practices. The non-dimensional conversion has been taken into account by the following operations:

$$X = \frac{x}{L_c}, Y = \frac{y}{L_c}, U = \frac{uL_c}{\alpha}, V = \frac{\mathrm{v}L_c}{\alpha}, P = \frac{pL_c^2}{\alpha^2\rho}, \\ \theta = \frac{T-T_C}{T_H-T_C}, Ra = \frac{g\beta(T_H-T_C)L_c^3}{\nu\alpha}, Pr = \frac{\nu}{\alpha} \quad (13)$$

After these conversion operations, the symbols *U* and *V* signify the dimensionless velocity components in dimensionless directions of *X* and *Y*, while L_c indicates the characteristic length, which is taken as the cavity height, *H*. The dimensionless temperature and pressure are denoted by θ and *P*, while the Rayleigh and Prandtl numbers are indicated by *Ra* and *Pr*. T_H and T_C respectively signify the hot and cold wall temperatures. Consequently, the non-dimensional forms of the above-given governing equations can be expressed via Eqs. 14–17. Furthermore, the thermal behavior of the fluid inside the various enclosures investigated was elaborated over dimensionless streamlines and temperature contours, as well as the *Nu*, which is computed regarding the ratio of the average heat flux in convection ($\dot{q}_{conv}$) to that in pure conduction case ($\dot{q}_{cond}$), as expressed in Eq. 18.

$$\frac{\partial U}{\partial X} + \frac{\partial \mathrm{V}}{\partial Y} = 0 \quad (14)$$

$$U\frac{\partial U}{\partial X} + V\frac{\partial V}{\partial Y} = -\frac{\partial P}{\partial X} + Pr\left(\frac{\partial^2 U}{\partial X^2} + \frac{\partial^2 U}{\partial Y^2}\right) \quad (15)$$

$$U\frac{\partial \mathrm{V}}{\partial X} + V\frac{\partial \mathrm{V}}{\partial V} = -\frac{\partial P}{\partial Y} + Pr\left(\frac{\partial^2 V}{\partial X^2} + \frac{\partial^2 V}{\partial Y^2}\right) + RaPr\theta \quad (16)$$

$$U\frac{\partial \theta}{\partial X} + V\frac{\partial \theta}{\partial Y} = \frac{\partial^2 \theta}{\partial X^2} + \frac{\partial^2 \theta}{\partial Y^2} \quad (17)$$

$$Nu = \frac{\dot{q}_{conv}}{\dot{q}_{cond}} \quad (18)$$

The boundary conditions implemented to solve the relevant governing equations include the no slip boundary condition applies at the wall surfaces, isothermal wall temperature that are hot (T_H) and cold temperatures (T_C) at the bottom and top walls of the enclosure, which can be respectively expressed by θ=1 and θ=0 in dimensionless form. The side walls of the enclosure are taken to be adiabatic. Although the present study is conducted in a dimensionless framework, it is worth noting that the Prandtl number of the fluid inside the enclosurre is *Pr*=2.99, which corresponds approximately to the thermophysical properties of water within the relevant temperature range.

Besides, the Rayleigh number considered within the study was varied by adjusting gravitational acceleration values.

2.2. Numerical Procedure

The governing equations explained in the previous section were solved under the relevant boundary conditions using a finite volume method-based solver. Second-order upwind scheme was considered for the discretization of the convective terms, while the coupling of pressure-velocity fields was handled by SIMPLE algorithm. The criteria for the convergence of the continuity, momentum and energy equations were specified to be 10^{-5}, 10^{-5}, and 10^{-8}, respectively. A structured face meshing suitable for the 2D geometry was considered within the present work. The number of mesh elements was determined by the number of equal divisions starting from the bottom wall. The elements were quadrilaterally dominant within the fluid domain, and the average aspect ratio was 1.62 for the geometry in Case V3. The minimum and average orthogonal quality values were 0.56 and 0.95, respectively, while the maximum skewness was 0.62. The solution has been ensured to be independent of the grid as a result of an attentive grid independence test. One of the most struggling case in terms of natural convective fluid flow, which is Case V3 at $Ra=10^6$, was selected for the grid independence test to ensure that the grid considered was undoubtedly sufficient for accurate solution. Consequently, five different grid divisions, namely 25×25, 33×33, 50×50, 100×100 and 150×150, have been tested, and the outcomes in terms of *Nu* exhibited negligible difference between the 100×100 and 150×150 structures, which indicated that using a grid structure of 100×100 is sufficient for the balance of accuracy and computational cost. The view of the mesh structure considered in this case was depicted in Figure 3a together with a scale-up portion, while the results of the grid independence test are illustrated in Figure 3b.

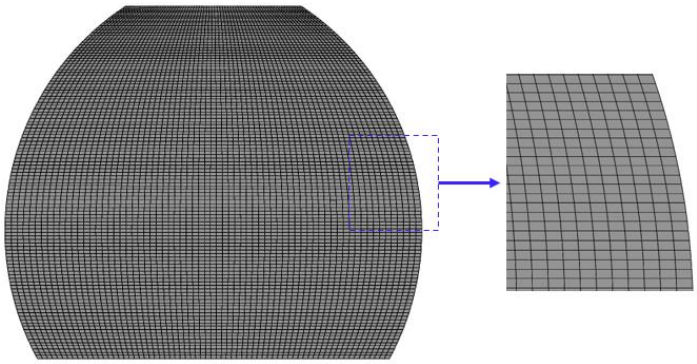

(a)

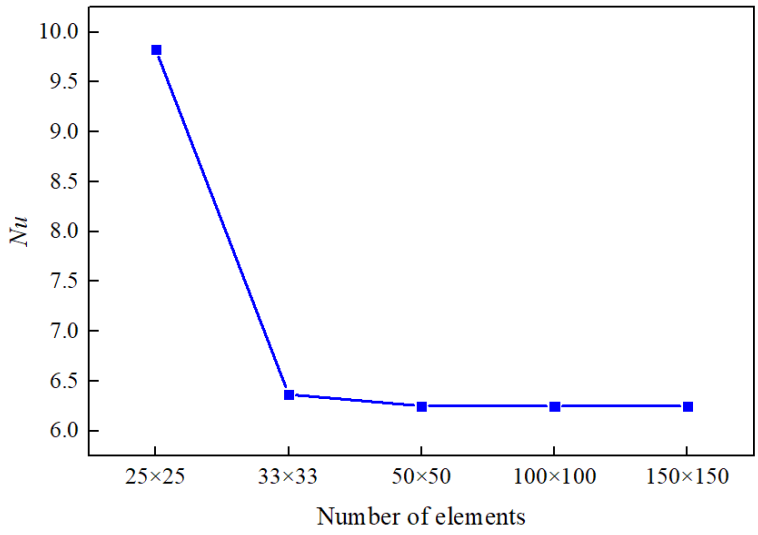

(b)

Figure 3. a) Exemplary schematic of the grid structure of Case V3, and b) outcomes of the grid independence test

The validity of the numerical procedure is ensured by an appropriate benchmark with the existing literature data on free convection in TEs. As a result of this benchmark that has been conducted against the study of Lasfer et al. [27] and depicted in Table 2, the highest discrepancy across the cases was computed to be 1.93%, which assures the credibility of the present work.

Table 2. Results of validation procedure

Rayleigh number	Nusselt number		
	Lasfer et al. [27]	Present study	Deviation
10^4	2.174	2.132	-1.94%
10^5	4.236	4.183	-1.26%
10^6	8.049	8.072	0.29%

3. RESULTS AND DISCUSSION

The flow structure and free convective heat transfer performance across the enclosure types investigated were comparatively discussed on dimensionless streamline and temperature contours, and they were quantified by *Nu*. In the following subsections, these performance parameters are respectively presented and discussed for each case examined within the framework of the study, in regard to different *Ra*.

3.1. Flow Structure and Temperature Distribution

Figure 4, 5, and 6 display the dimensionless streamline and temperature contours with respect to various *Ra*. In Figure 4, focused on the thermal behavior of the fluid at $Ra=10^4$, it was evidently noticed that the concave structure of the enclosures led to the occurrence of separated circulation zones, particularly for the enclosures of C2 and C3 where the wall curvature is relatively higher. This phenomenon can be attributed to the restricted flow region for the fluid inside the enclosure. As the geometry of the flow field was narrowed down, the fluid flow was hindered, and the effect of buoyancy forces was diminished. Therefore, separated circulation zones occurred, which triggered a relatively more stratified temperature distribution, as seen from the isotherms. While a relatively non-uniform temperature distribution was noted for the reference cavity and C1, the isotherms exhibited a more stratified temperature distribution in vertical direction within the enclosure, indicating a conduction-dominant heat transfer. Comparing the reference geometry, which is the standard TE, and the C1, the penetration of cold fluid through the middle section of the enclosure is more noticeable in the reference case.

On the other hand, the convex geometries, namely V1, V2, and V3, demonstrated an enlarged flow circulation in parallel with the outward curved side walls. According to the streamline and corresponding isotherms, it was seen that the buoyancy-driven fluid flow is strengthened as the curvature of the walls are increased through outward, compared to the standard trapezoidal case, and a larger mixing occurs between the thermally active walls.

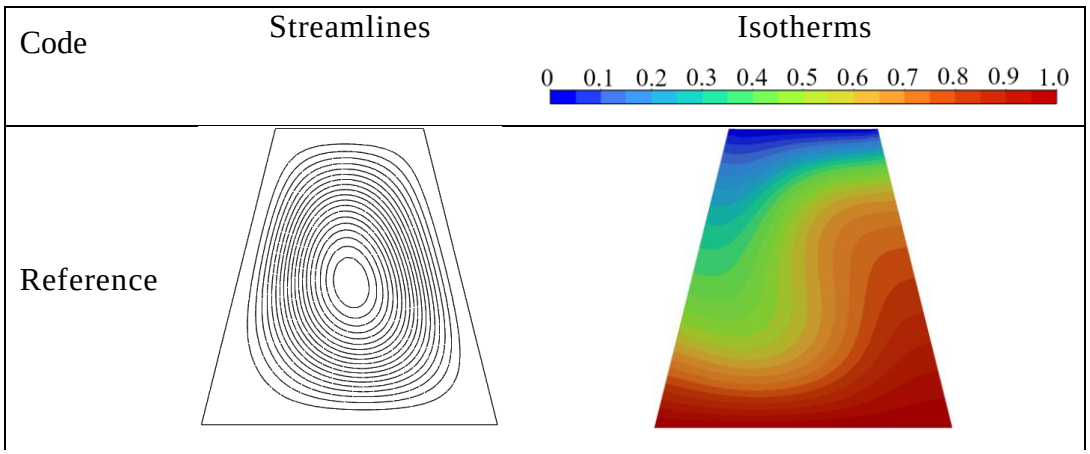

C1	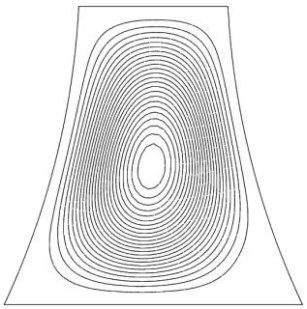	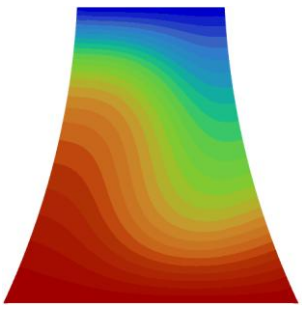
C2	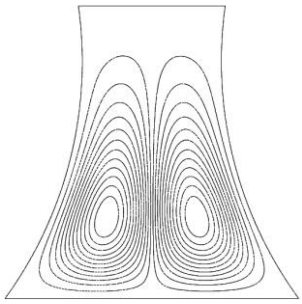	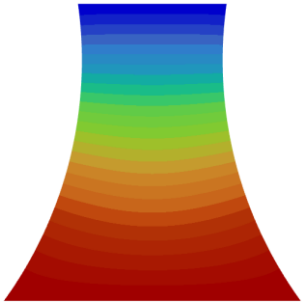
C3	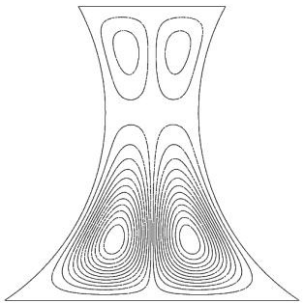	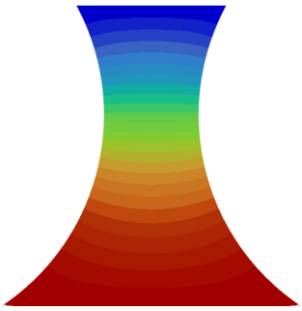
V1	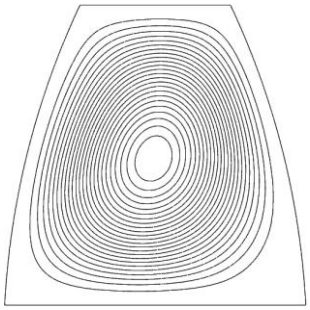	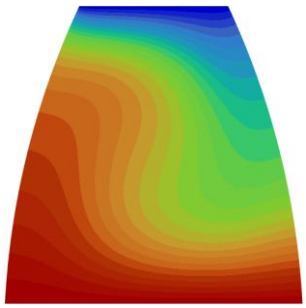
V2	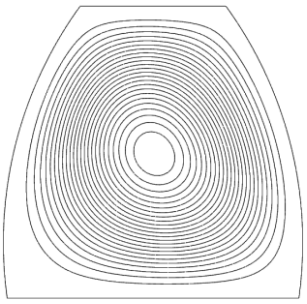	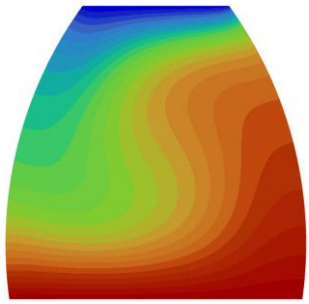

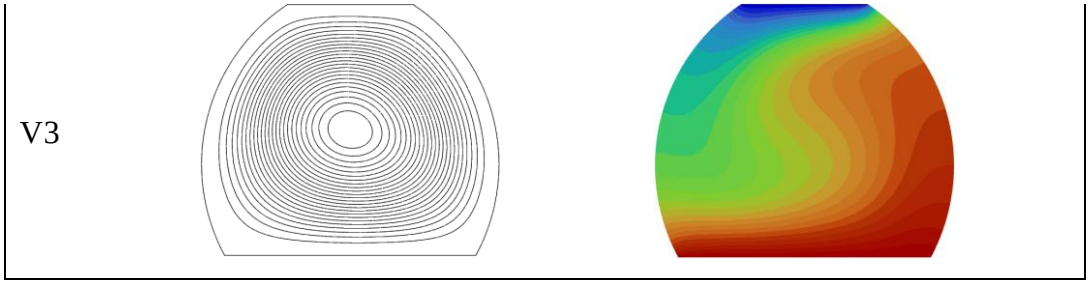

Figure 4. Dimensionless streamline and isotherm contours at $Ra=10^4$ for the concave and convex geometries investigated

The dimensionless streamline and temperature variations were demonstrated for $Ra=10^5$ in Figure 5. Unlike the previous discussion, the augmentation in *Ra* resulted in stronger and divided fluid circulation zones in all cavities investigated, due to increased buoyancy forces. In the reference cavity and the convex shaped enclosures, namely V1, V2, and V3, two nearly symmetrical free convective circulation regions were formed. Thereby, an inverse mushroom shaped temperature contour was observed in these cases. More frankly, the fluid warmed up at the bottom wall rose up along the side walls through the cold top wall of the enclosure, and then the cooled-down fluid descended down the symmetrical axis of the enclosure in the middle section. Nevertheless, for the concave shaped enclosures (C1, C2, and C3), the circulation zones were seen to be formed in the upper and lower regions of the enclosure, which consequently restricted the relatively hot fluid portions to effectively contact the cold wall to increase the convective heat transfer coefficient along the thermally active walls. Furthermore, dead flow regions were formed, and the fluid in these regions could not contribute to thermal transport, leading to a significant decrement in free convection. The corresponding isotherms confirmed the aforementioned influence of fluid flow on the heat transfer. As seen from the figure, the hot and cold fluid regions accumulated separately in the lower and upper parts of the cavity, respectively, and remained stratified, especially for C1 and C2, at this *Ra*.

Code	Streamlines	Isotherms 0 0.1 0.2 0.3 0.4 0.5 0.6 0.7 0.8 0.9 1.0
Reference	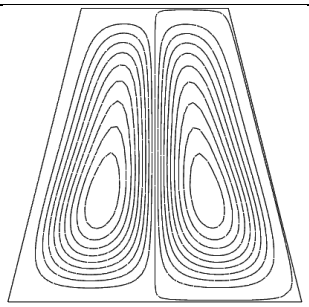	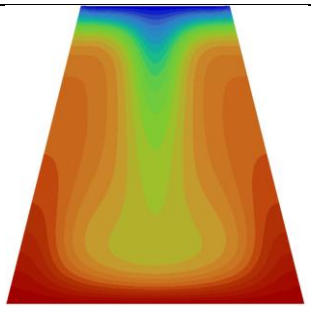
C1	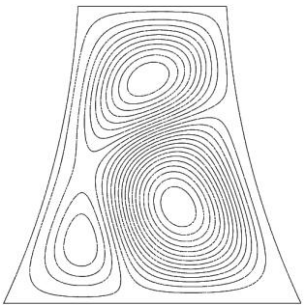	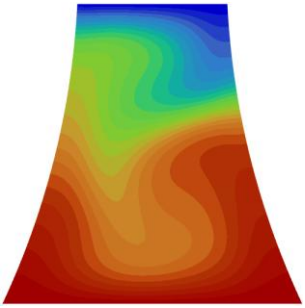
C2	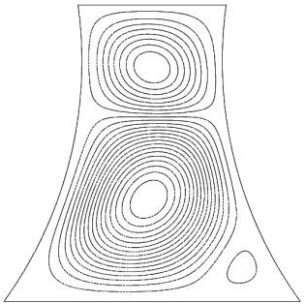	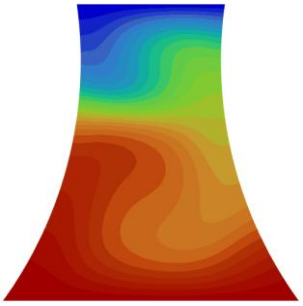
C3	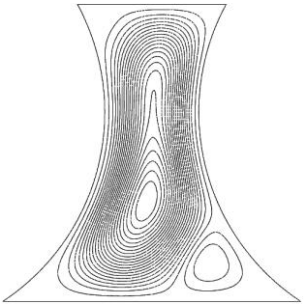	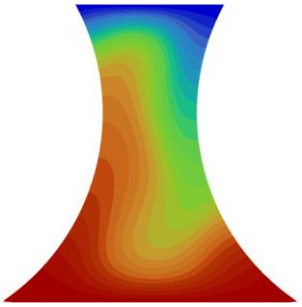
V1	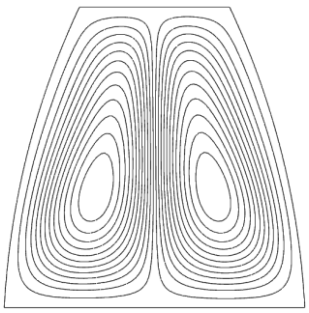	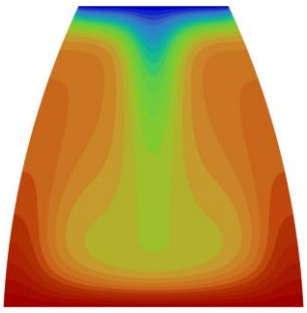

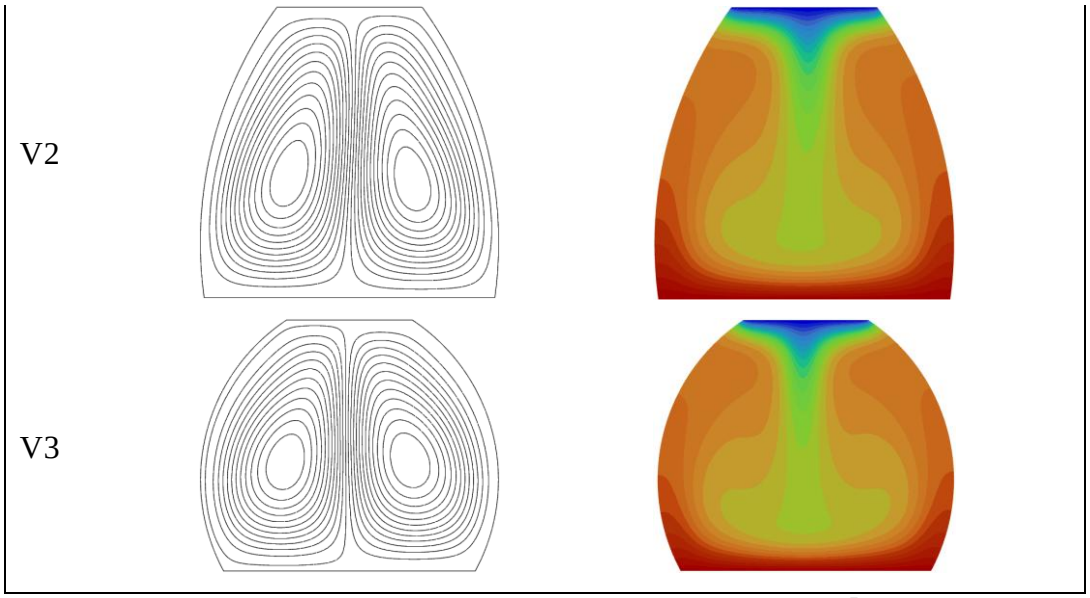

Figure 5. Dimensionless streamline and isotherm contours at $Ra=10^5$ for the concave and convex geometries investigated

When *Ra* increased to $Ra=10^6$, the pattern of the streamline and isotherms significantly varied, compared to previous *Ra* examined, as seen from Figure 6. As the buoyancy forces are remarkably stronger at this *Ra*, there were several natural convection vortices formed in various regions of the enclosure. Especially for the reference case and the concave cases (C1, C2, and C3), these vortices were noticed to be asymmetrical. Nonetheless, the displacement and region-swap of the hot and cold fluid streams were relatively more restricted for C1 and C2, compared to other enclosures investigated. Similar to the previous discussions, in the middle section with respect to *y*-axis, the free convective fluid flow and heat exchange became weaker in these enclosures. Hence, the thermal coupling between the hot and cold fluids remained insufficient.

In the convex cavities, on the other hand, there were one or two circulation zones observed. For V1 and V2, two asymmetrical and relatively larger (compared to concave ones) vortices developed along the vertical axis within the enclosures. Thereby, the warmed-up fluid flowed upwards in V1 and V2 along the convex side walls, and then it flowed along the middle section directly downwards. However, for V3, a more circular fluid flow was observed by the outcomes, i.e., the hot fluid rose up along the left wall, cooled down along the top wall and then descended along the right wall.

Code	Streamlines	Isotherms
		0 0.1 0.2 0.3 0.4 0.5 0.6 0.7 0.8 0.9 1.0
Reference	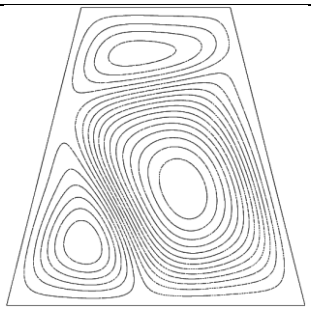	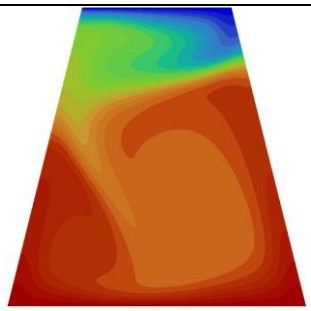
C1	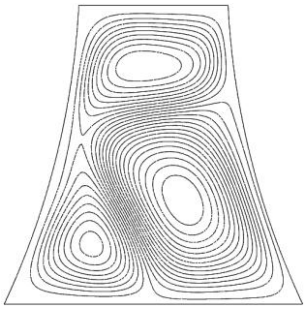	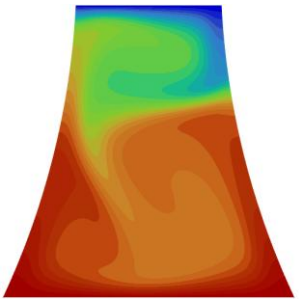
C2	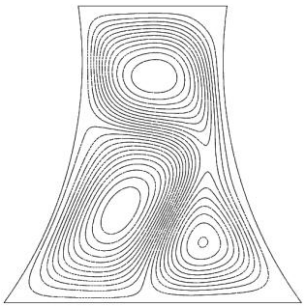	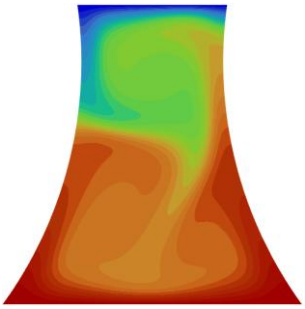
C3	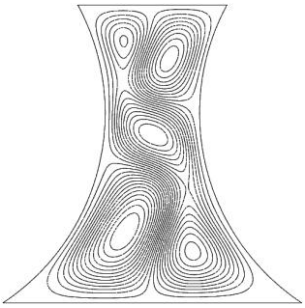	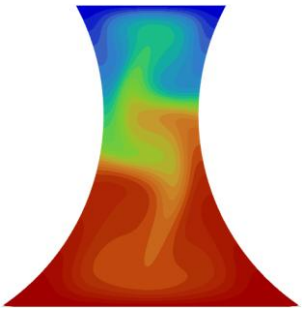
V1	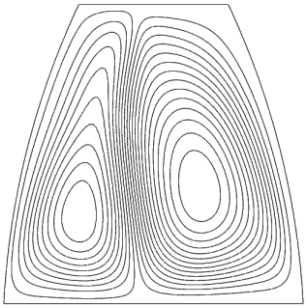	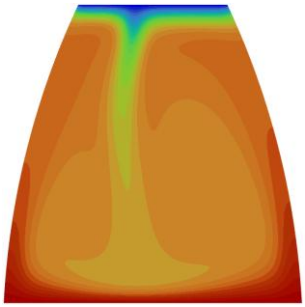

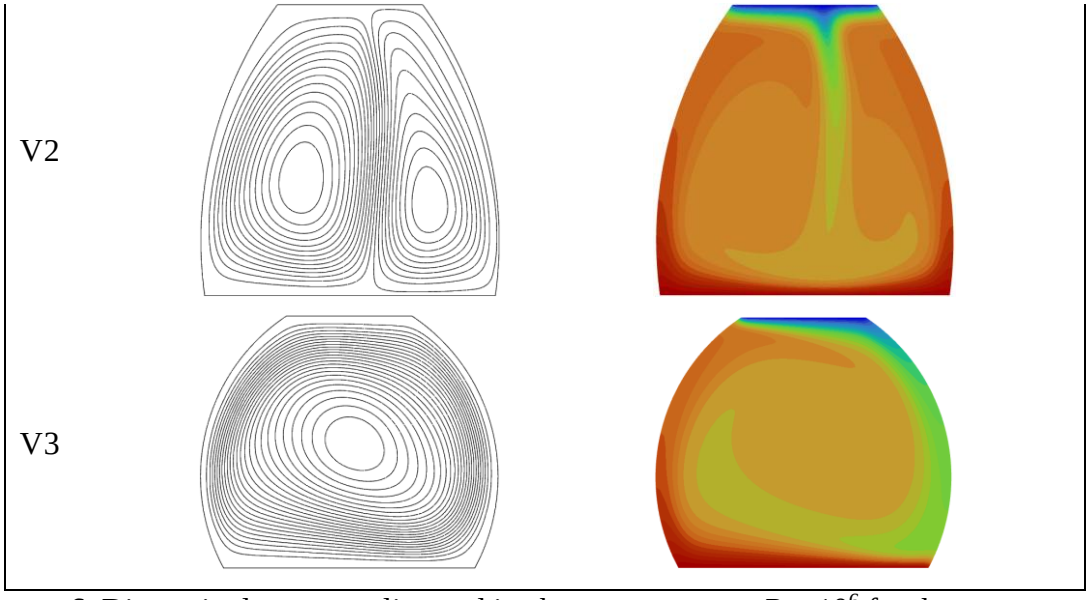

Figure 6. Dimensionless streamline and isotherm contours at Ra=10^6 for the concave and convex geometries investigated

3.2. Nusselt Numbers

Average Nusselt numbers were presented in Figure 7 and 8 for the quantification of the natural convection effect as well as for the comparison of the geometric influences on the thermal transport. The influence of concave enclosure geometry on *Nu* is compared to the reference TE, and the outcomes are accordingly discussed over Figure 7, for the *Ra* investigated.

At first sight, the *Nu* are considerably lower for the concave TEs at Ra=10^4 and 10^5, compared to the reference case, which is a standard isosceles TE. Yet, the *Nu* for the C2 was found to be almost the same as the reference case at Ra=10^6. Quantitative results demonstrated that the average Nusselt number at Ra=10^4 was computed to be 1.83 for the reference case, while it was 1.57 for C1, and it was even unity for C2 and C3. Compared to the reference enclosure, the *Nu* in the cavities of C1, C2, C3 were respectively 14%, 45%, and 45% lower, which indicates a significant reduction in free convective heat transfer, and the mechanism is even pure-conduction for the enclosures C2 and C3. A similar observation was noted at Ra=10^5, and the *Nu* values were 3.83, 3.02, 2.14, and 3.45 for the reference case, C1, C2, and C3, respectively. Related to the previous discussion, the squeezing of the enclosure restricted the fluid motion, hence, it led to considerable thermal stratification.

However, at Ra=10^6, an exception was observed where the Nu for the reference enclosure and C2 were found to be almost identical. On the other hand, C1 and C3 yielded significantly lower values. This can be attributed to the well-mixing of fluid in the enclosure C2, while it was stuck in C3 with a high thermal stratification and local circulation zones damping each other in C1, as previously shown in Figure 6. Nu computed for these cases were 6.25 for the reference case, and 5.16, 6.26, and 4.77 for C1, C2, and C3, respectively. This indicates that Nu decreased by 17.5% and 23.7% for the enclosures C1 and C3, respectively, compared to the standard isosceles TE.

To sum up, modifying the side walls of standard TEs in a concave way is not recommended as a heat transfer enhancement technique, due to the damping effect on the natural convective flow and high thermal stratification, which hinders the effective heat exchange by decreasing local temperature gradients.

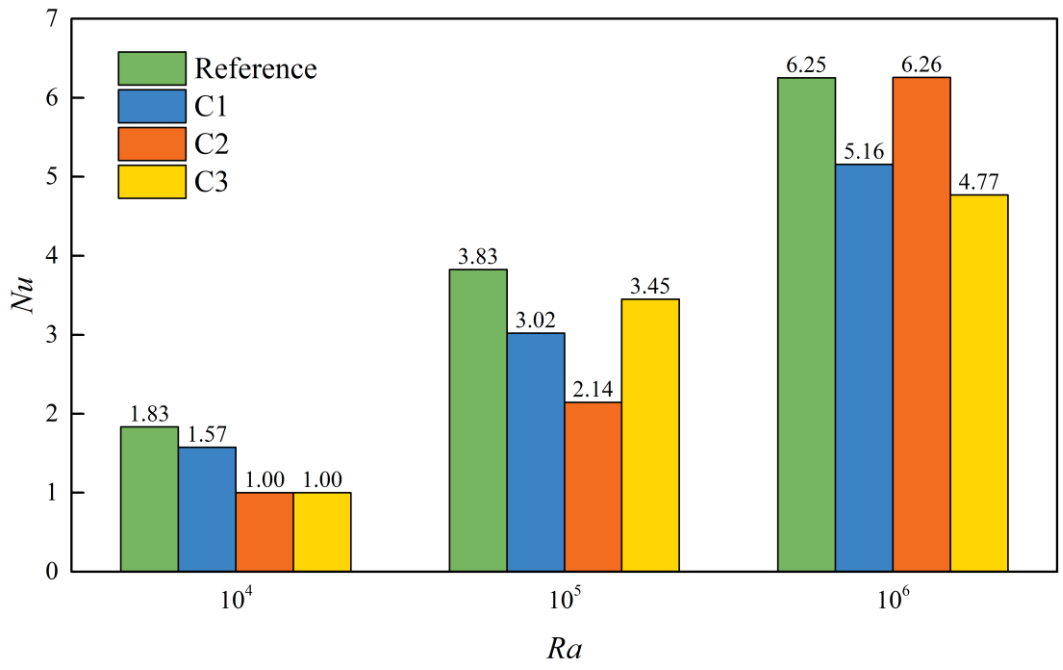

Figure 7. Nu values for the reference and concave enclosures at different Ra.

Figure 8 depicts the variation of Nu with respect to different Ra for the reference and the convex shaped enclosures. Unlike the concave enclosures, the Nu exhibit a superior trend compared to the reference case, particularly at the low and high Ra investigated. At Ra=10^4, the Nu computed were 1.83, 1.99, 2.07, and 2.17 for the reference, V1, V2, and V3, respectively. This shows that a notable increase occurred as the curvature of the side walls increased, and the enhancement rates in Nu with respect to reference enclosure were calculated to be 8.3%, 13.1% and 18.6% for the V1, V2,

and V3, respectively. Parallel to the deduction made from the streamline and isotherm contours, the convex curvature of the side walls enabled smoother and stronger free convective circulation of the fluid inside the domain. Thereby, this geometric modification became helpful for the boosting of the buoyancy forces.

Nevertheless, as the buoyancy forces are already increased up to a specific level when *Ra* is switched to $Ra=10^5$, this advantage of the curved walls has diminished. As seen from the relevant contours in Figure 5, the hot fluid arisen along the side walls contacted the cold wall and the cooled-down fluid descended through the middle section of the enclosure, making an inverse mushroom shape temperature contour. This phenomenon was a common occurrence for all the enclosure investigated, regardless of the wall curvature. Therefore, the *Nu* computed for these cases yielded almost the same values, namely 3.83, 3.82, 3.78 and 3.73 for the reference, V1, V2, and V3, respectively, where the maximum discrepancy was 2.4% (between the reference and V3 enclosures).

At the highest *Ra* examined ($Ra=10^6$), the differences in *Nu* became more noticeable, particularly for the enclosures V1 and V2, while there was a marginal difference between the reference case and the V3. Quantitative findings showed that the *Nu* values calculated for the reference case, V1, V2, and V3 enclosures were respectively 6.25, 6.81, 6.83, and 6.23. Hence, V1 and V2 achieved an enhancement of 8.9% and 9.3%, respectively, compared to the reference case. Related to the fluid flow behavior, this result is attributed to the double circulation zones along the two side walls in the enclosures V1 and V2, while there was only one single circulation in V3. Because the hot fluid rising up through two branches along the convex shaped side walls met up at around the midpoint of the cold wall, and then the cooled down fluid descended down through the middle section of the enclosure, which ensured a more effective mixing of hot and cold portions of the fluid. On the other hand, V3 exhibited a single circulation of the heated fluid from bottom to top in clockwise direction, hence, a relatively poorer fluid mixing occurred, which resulted in weaker convection currents. Lastly, in the reference case, although there were a few different circulation zones, these have blocked each other and restricted the mixing of hot and cold fluid portions, resulting in relatively lower *Nu* as well.

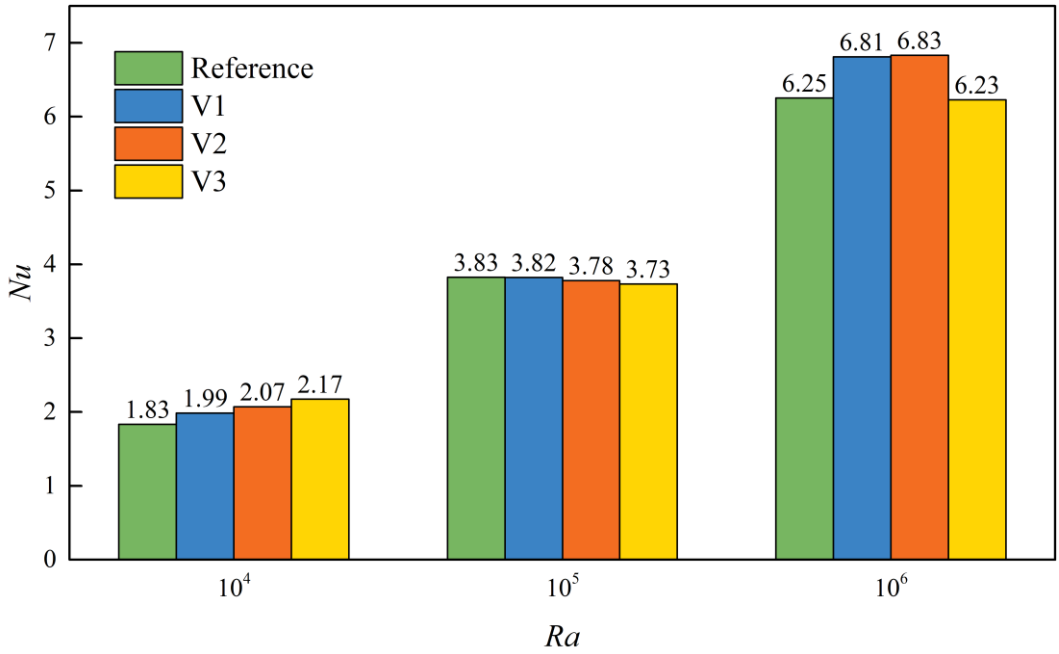

Figure 8. *Nu* values for the reference and convex enclosures at different *Ra*.

4. CONCLUSION

The impact of side wall curvature of a basically isosceles TE on the natural convective flow and heat transfer characteristics of the fluid inside have been explored within this work. For this purpose, apart from the reference case involving standard isosceles TE, three different concave (abbreviated as C1, C2, and C3) and three different convex shaped (abbreviated as V1, V2, and V3) cavities were taken into consideration. Furthermore, three different *Ra* (namely, $Ra=10^4$, 10^5, and 10^6) were considered to numerically elaborate the natural convection effects at different buoyancy force strengths.

The geometrical modification considered within the study led to significant variations in fluid flow, temperature distribution and consequently in Nusselt numbers. The major conclusions drawn from the work are presented as follows:

- Concave type enclosures led to the formation of squeezed and separated circulation zones within the enclosure, and this formation resulted in dead-circulation zones, and the separated local vortices restricted the mixing of hot and cold fluid portions, which consequently decreased the natural convection effects.

- In the convex enclosures, on the other hand, the fluid circulation became stronger, particularly for Ra=10^5 and 10^6, and the formation of two asymmetrical vertical, i.e., longitudinal, vortices allowed a more effective fluid mixing due to the fact that the heated-up fluid rose up through side walls and descended down through the middle section, which enabled higher local temperature gradients.

- The wall curvature has a significant impact on the alteration of natural convective fluid flow. Concave shaped enclosures were insufficient for enhancing the natural convection, while convex cavities were superior to the reference standard isosceles TE, particularly at relatively lower Ra.

- Quantitative outcomes showed that concave enclosures had a significant adverse impact restricting the natural convective fluid flow, and the average Nusselt number can decrease by up to 45%, compared to the reference enclosure, at low Ra, and the thermal stratification increased in this enclosure.

- Depending on the Ra, convex enclosures exhibited a considerable enhancement effect on the natural convection. Especially at low Ra (Ra=10^4), the improvement in Nu can reach up to 18.6%, compared to the reference enclosure, while this ratio was found to be 9.3% at the highest Ra examined. Nevertheless, due to the balance between the buoyancy forces and the geometrical effects, the improvement impact was diminished at the moderate Rayleigh number.

To conclude, a simple geometrical modification on a standard isosceles TE was found to be significantly beneficial in terms of natural convective heat transfer enhancement when the design and operational conditions were accordingly considered. Therefore, it can be recommended to consider convex trapezoidal shaped enclosures to boost the natural convection in engineering applications such as cooling of electronic devices, solar thermal energy harvesting and relevant heat exchangers, with a relatively cost-effective method.

NOMENCLATURE

C_p	Specific heat (J kg^{-1} K^{-1})
g	Gravitational acceleration (m s^{-2})

H	Enclosure height (m)
k	Thermal conductivity ($Wm^{-1}K^{-1}$)
L_c	Characteristic length (m)
Nu	Average Nusselt number
p	Fluid pressure (Pa)
P	Dimensionless fluid pressure
Pr	Prandtl number
Ra	Rayleigh number
T	Temperature (K)
t	Dimensionless arc parameter
u	Horizontal velocity component ($m\ s^{-1}$)
U	Horizontal component of dimensionless velocity
v	Vertical velocity component ($m\ s^{-1}$)
V	Vertical component of dimensionless velocity
x,y	Cartesian coordinates (m)
X,Y	Dimensionless coordinates

Subscripts

C	Cold
H	Hot
ref	Reference

Greek letters

α	Thermal diffusivity ($m^2\ s^{-1}$)
β	Coefficient of thermal expansion (K^{-1})
θ	Temperature in dimensionless form
μ	Dynamic viscosity ($kg\ m^{-1}\ s^{-1}$)
ν	Kinematic viscosity ($m^2\ s^{-1}$)
φ	Polar angle (rad)
ρ	Fluid density ($kg\ m^{-3}$)

ACKNOWLEDGMENT

No financial support was received for the research, authorship, and/or publication of this article.

DECLARATION OF ETHICAL STANDARDS

No ethical committee approval and/or legal or special permission was required for the conduct of this study.

CONTRIBUTION OF THE AUTHORS

Çağatay Yıldız: Conceptualization, Methodology, Software, Validation, Formal analysis, Investigation, Data curation, Visualization, Writing – Original draft, Writing – Review & Editing.

CONFLICT OF INTEREST

No conflict of interest was identified in this study.

REFERENCES

[1] Kandeal AW, Ismail M, Basem A, Elsayad MM, Alawee WH, Majdi HS, Abdullah AS, Jang SH, An M, Omara ZM, Ghazaly NM, Sharshir SW. An overview of the improvement of natural convection heat transfer via surface thermal radiation for different geometries. Results in Engineering 2024; 23: 102514.

[2] Hussain Z, ul ain N, Ullah N, Nisar Z, Anwar MS. Influences of natural convection on cylindrical objects within a square enclosure with varied shapes. Case Studies in Thermal Engineering 2025; 74: 106772.

[3] Rahimi A, Dehghan Saee A, Kasaeipoor A, Hasani Malekshah E. A comprehensive review on natural convection flow and heat transfer. International Journal of Numerical Methods for Heat and Fluid Flow 2019; 29: 834–877.

[4] Venkatadri K, Anwar Bég O, Rajarajeswari P, Ramachandra Prasad V. Numerical simulation of thermal radiation influence on natural convection in a trapezoidal enclosure: Heat flow visualization through energy flux vectors. International Journal of Mechanical Sciences 2020; 171: 105391.

[5] Tayebi T, Öztop HF. Entropy production during natural convection of hybrid nanofluid in an annular passage between horizontal confocal elliptic cylinders. International Journal of Mechanical Sciences 2020; 171: 105378.

[6] Al-Mudhafar AHN, Nowakowski AF, Nicolleau FCGA. Performance enhancement of PCM latent heat thermal energy storage system utilizing a modified webbed tube heat exchanger. Energy Reports 2020; 6: 76–85.

[7] Giwa SO, Sharifpur M, Ahmadi MH, Meyer JP. Magnetohydrodynamic convection behaviours of nanofluids in non-square enclosures: A comprehensive review. Mathematical Methods in the Applied Sciences 2020; https://doi.org/10.1002/mma.6424.

[8] Bawazeer SA, Alsoufi MS. Natural convection in a square cavity: Effects of Rayleigh and Prandtl numbers on heat transfer and flow patterns. Case Studies in Thermal Engineering 2025; 73: 106680.

[9] Afsana S, Molla MM, Nag P, Saha LK, Siddiqa S. MHD natural convection and entropy generation of non-Newtonian ferrofluid in a wavy enclosure. International Journal of Mechanical Sciences 2021; 198: 106350.

[10] Parvin S, Chamkha AJ. An analysis on free convection flow, heat transfer and entropy generation in an odd-shaped cavity filled with nanofluid. International Communications in Heat and Mass Transfer 2014; 54: 8–17.

[11] Yıldız Ç, Yıldız AE, Arıcı M, Azmi NA, Shahsavar A. Influence of dome shape on flow structure, natural convection and entropy generation in enclosures at different inclinations: A comparative study. International Journal of Mechanical Sciences 2021; 197: 106321.

[12] Miroshnichenko IV, Sheremet MA, Oztop HF, Abu-Hamdeh N. Natural convection of Al2O3/H2O nanofluid in an open inclined cavity with a heat-generating element. International Journal of Heat and Mass Transfer 2018; 126: 184–191.

[13] Ji C, Qin Z, Dubey S, Choo FH, Duan F. Simulation on PCM melting enhancement with double-fin length arrangements in a rectangular enclosure induced by natural convection. International Journal of Heat and Mass Transfer 2018; 127: 255–265.

[14] Mahdi JM, Nsofor EC. Melting enhancement in triplex-tube latent thermal energy storage system using nanoparticles-fins combination. International Journal of Heat and Mass Transfer 2017; 109: 417–427.

[15] Kumar S, Mahapatra SK. Natural convection in open square enclosure with different heat source sizes. Heat Transfer Engineering 2024; 45: 1190–1205.

[16] Mote Gowda KGB, Rajagopal MS, Aswatha, Seethramu KN. Numerical studies on natural convection in a trapezoidal enclosure with discrete heating. Heat Transfer Engineering 2020; 41: 595–606.

[17] Natarajan E, Basak T, Roy S. Natural convection flows in a trapezoidal enclosure with uniform and non-uniform heating of bottom wall. International Journal of Heat and Mass Transfer 2008; 51: 747–756.

[18] Hemmat Esfe M, Abbasian Arani AA, Yan WM, Ehteram H, Aghaie A, Afrand M. Natural convection in a trapezoidal enclosure filled with carbon nanotube–EG–water nanofluid. International Journal of Heat and Mass Transfer 2016; 92: 76–82.

[19] Rahaman MM, Bhowmick S, Saha SC. Thermal performance and entropy generation of unsteady natural convection in a trapezoid-shaped cavity. Processes 2025; 13: 921.

[20] Rahaman MM, Bhowmick S, Saha SC. Unsteady natural convection and entropy generation in thermally stratified trapezoidal cavities: A comparative study. Processes 2025; 13: 1908.

[21] Rahaman MM, Bhowmick S, Pada Ghosh B, Xu F, Nath Mondal R, Saha SC. Transient natural convection flows and heat transfer in a thermally stratified air-filled trapezoidal cavity. Thermal Science and Engineering Progress 2024; 47: 102377.

[22] Bilal S, Rehman M, Noeiaghdam S, Ahmad H, Akgül A. Numerical analysis of natural convection driven flow of a non-Newtonian power-law fluid in a trapezoidal enclosure with a U-shaped constructal. Energies 2021; 14: 5355.

[23] Mehryan SAM, Ghalambaz M, Kalantar Feeoj R, Hajjar A, Izadi M. Free convection in a trapezoidal enclosure divided by a flexible partition. International Journal of Heat and Mass Transfer 2020; 149: 119186.

[24] Selimefendigil F. Natural convection in a trapezoidal cavity with an inner conductive object of different shapes and filled with nanofluids of different nanoparticle shapes. Iranian Journal of Science and Technology, Transactions of Mechanical Engineering 2018; 42: 169–184.

[25] Prince HA, Rozin EH, Sagor MJH, Saha S. Evaluation of overall thermal performance for conjugate natural convection in a trapezoidal cavity with different surface corrugations. International Communications in Heat and Mass Transfer 2022; 130: 105772.

[26] Dutta S, Kumar P, Kalita JC. Streamfunction-velocity computation of natural convection around heated bodies placed in a square enclosure. International Journal of Heat and Mass Transfer 2020; 152: 119550.

[27] Lasfer K, Bouzaiane M, Lili T. Numerical study of laminar natural convection in a side-heated trapezoidal cavity at various inclined heated sidewalls. Heat Transfer Engineering 2010; 31: 362–373.